Causin and Malgaroli *Journal of Mathematics in Industry* (2016) 6:9
DOI 10.1186/s13362-016-0031-7

Journal of Mathematics in Industry
a SpringerOpen Journal

RESEARCH Open Access

Mathematical assessment of drug build-up in the posterior eye following transscleral delivery

Paola Causin[1*] and Francesca Malgaroli[2]

*Correspondence:
paola.causin@unimi.it
[1]Dipartimento di Matematica, Università degli Studi di Milano, Milano, Italy
Full list of author information is available at the end of the article

Abstract

Delivery of drugs to the posterior segment of the eye is a significant challenge in the field of opthalmic pharmaceuticals. Several restrictive barriers hinder drug delivery to this district. Static barriers include tissues and limiting membranes, while dynamic barriers include drug clearance mechanism from blood and lymphatics. Strategies for delivering drugs to the posterior segment most often consist in topical ocular medications or systemic administrations, but dose/response profiles are generally very poor. Intravitreal injections and transscleral delivery are new emerging techniques with promising results. Purpose of this study is to develop a mathematical model to assess drug levels subsequent to a transscleral drug implant. Both computational and analytical techniques are adopted. The model comprises sclera, choroid, retina and vitreous along with the retina pigment epithelium at the choroid-retina boundary and the inner blood retinal barrier of the retinal vessels. Darcy equations are used to compute the filtration velocity of the interstitial fluid and a fictitious velocity field is added to model active pumping from the retinal pigmented epithelium. Convective-diffusive-reactive equations for drug concentration are then solved. Permeability parameters and partition coefficients simulate the presence of internal membranes and barriers, with possible different values in outward and inward directions. An important result of the model is the evaluation of the roles of the different physical parameters, which offers key points to improve drug delivery techniques. Namely, the sensitivity study suggests that diffusion in tissue, clearance rates, membrane permeabilities and active pumping play important roles in determining drug peak concentration and time-to-peak. However, their relative influence can be dramatically different depending on the rate-limiting parameter.

Keywords: ocular drug delivery; RPE active pumping; blood retinal barrier; ocular membrane permeability; mathematical model

1 Introduction

The understanding of drug delivery mechanisms in the posterior segment of the eye (PSE) - including sclera, choroid and retina - is one of the most challenging tasks in the pharmaceutical industry [1]. The efficiency of drug delivery to the PSE is hindered by several barriers. Static barriers consist of physical obstacles to drug diffusion such as the sclera itself, the retinal pigment epithelium (RPE, the so-called outer blood retinal, oBRB) and

© 2016 Causin and Malgaroli. This article is distributed under the terms of the Creative Commons Attribution 4.0 International License (http://creativecommons.org/licenses/by/4.0/), which permits unrestricted use, distribution, and reproduction in any medium, provided you give appropriate credit to the original author(s) and the source, provide a link to the Creative Commons license, and indicate if changes were made.

the retinal vessels (the so-called inner blood retinal barrier, iBRB). Dynamic barriers include drug clearance mechanisms through blood and lymphatic vessels and degradation processes. Drug solubility, lipophilicity, charge, degree of ionization, molecular size and shape affect the penetration rate of the drug across the various barriers [2]. Convection by interstitial fluid filtration can play a certain role especially when considering low-diffusible molecules [3]. There is also considerable evidence suggesting that active transport ('pumping') across the RPE can induce significant effects, sucking out fluid, and thus dissolved drugs, from the retina towards the choroid [4, 5].

Literature on mathematical models of the pharmacokinetics of ocular and periocular delivery systems is relatively sparse (see Chapter 4 of [6] for a recent review on this subject). Table 1 presents - at the best of our knowledge - a schematic survey of the existing most recent mathematical models of ocular drug delivery. There is a general agreement in distinguishing between small (molecular weight < 1 kDa, as fluoroscein) and large (molecular weight > 10 kDa, as albumin, antibodies) molecules, since they display different diffusivities. Interstitial fluid filtration is also kept into account in several papers by Darcy equations, under the hypothesis of steady flow. Interface boundary conditions for the drug concentration between different subdomains (vitreous, retina, choroid, sclera or combi-

Table 1 Schematic prospect of existing mathematical models in recent literature on ocular drug delivery

	sub–domains				filtration field				blood phase			
Reference	V	R	C	S	V	R	C	S	V	R	C	S
Kavousanakis et al. [17], 3D	✓	✓	✓		✓	✓	✓				✓	
Kotha et al. [21], 3D	✓	✓	✓	✓			✓					
Stay et al. [7], 3D	✓				✓							
Tojo [29], 3D	✓											
Kim et al [30], 3D	✓	✓			✓	✓						
Ninawe et al. [12], 0D		✓	✓	✓								
Balachandran et al. [8], 3D	✓	✓	✓		✓	✓	✓				✓	
Missel at al. [20],3D	✓	✓	✓	✓	✓	✓	✓	✓				
Mac Gabhann et al. [13], 1D		✓	✓	✓								
Amrite et al. [9], 0D		✓	✓							✓		
Park et al. [31], 3D	✓	✓			✓[d]	✓[d]	✓[d]					

	active pumping				interface bcs for drug			molecule weight	
Reference	V	R	C	S	V-R	R-C	C-S	small	large
Kavousanakis et al. [17], 3D		✓[a]						✓	✓
Kotha et al. [21], 3D		✓[b]			✓[c]	✓[c]	✓[c]	averaged	
Stay et al. [7], 3D	✓[b]				✓			✓	✓
Tojo [29], 3D					✓			✓	
Kim et al. [30], 3D									✓
Ninawe et al. [12], 0D					✓	✓	✓		✓
Balachandran et al. [8], 3D		✓[a]						✓	
Missel at al. [20],3D								✓	✓
Mac Gabhann et al. [13], 1D					✓[c]	✓[c]	✓[c]	✓	✓
Amrite et al. [9], 0D						✓			✓
Park et al. [31], 3D		?						✓	✓

Symbols: nD, $n = 0, 1, 3$: spatial dimensions of the model; V = vitreous, R = retina, C = choroid, S = sclera. [a]: treated with an addictional fictitious advective term; [b]: treated with different inward and outward membrane permeabilities. Merged cells in a row indicate that the corresponding domains are treated as a sole entity. Interface boundary conditions are checked when a Robin-type boundary conditions with a specific membrane permeability is used for drug at interface; [c]: a partition coefficient is considered at the interface; [d]: Navier-Stokes equations are considered.

nations of them) are assigned via simple continuity of normal fluxes or via more complex Robin-type conditions modeling the presence of a permeable membrane. More controversial, less investigated, points are represented by the inclusion of active transport mechanisms (see [7, 8]) and the interaction of the drug with blood flow in circulatory vessels (see [8, 9]). These latter aspects turn out to be very relevant when computing drug levels in the retina after periocular administration. The retina is an important therapeutic target but only a few studies address it specifically (refer to Table 1). The present paper aims at addressing this topic. We present a 1D model including vitreous, retina, choroid and sclera subdomains with a blood phase in the retina. We compute the filtration velocity of the interstitial fluid and we solve convective-diffusive-reactive equations for drug concentration. Permeability parameters and partition coefficients simulate the presence of internal membranes and barriers. We carry out numerical simulations based on transscleral drug delivery, which is an attractive alternative to the intravitreous mode of administration. We investigate the problem sensitivity with respect to the above mentioned parameters, which allow to evaluate the importance of tuning these properties when devising a new drug and their relative importance.

The paper is organized as follows. In Section 2, we present the geometrical assumptions and the mathematical model of the PSE. In Section 3, we show the results obtained from numerical solution of the mathematical model and sensitivity analysis. In Section 4, we discuss the significance of the model and the main results relevant for devising new drug formulations and delivery techniques. Eventually, in Section 4, we draw the conclusions of the work. A theoretical analysis is carried out in the Appendix to establish lower and upper bounds for the drug concentration in the retina, an important target for drug delivery.

2 Mathematical model of the posterior segment of the eye

2.1 Geometrical description of the PSE

Compartmental models of the PSE have been presented in [10–12] to describe drug administration via a subconjunctival application or an episcleral hydrogel implant. Consensus has been reached about the necessity of including separate compartments which represent the different anatomical structures in the PSE. In [9], a study has been carried out to evaluate the compartment subdivision which provides the best fitting of experimental data. The most effective identified configuration includes compartments representing site of drug release, periocular tissue, sclera/choroid/RPE, retina and a non-specified distribution compartment. An analogous identification of relevant independent structures is carried out in [13], where a 1D continuum model describes levels of fluoroscein after periocular administration.

According to the above arguments, we model the PSE as the union of four different layers, treated as 1D slabs (see Figure 1), representing:

- *sclera* (S), an avascular and largely acellular coat of extracellular matrix relatively permeable to molecules;
- *choroid* (C), a dense network of large and small blood vessels with a relatively sparse population of cells;
- *retina* (R), composition of several layers of densely packed neuronal and glial cells, vascularized by arterioles and venules which run superficially along the retinal inner surface and supply/drain the embedded capillary plexi (see Figure 2, top panel);
- *vitreous* (V), a clear, avascular, gelatinous body which accounts for about 80% of the volume of the eye.

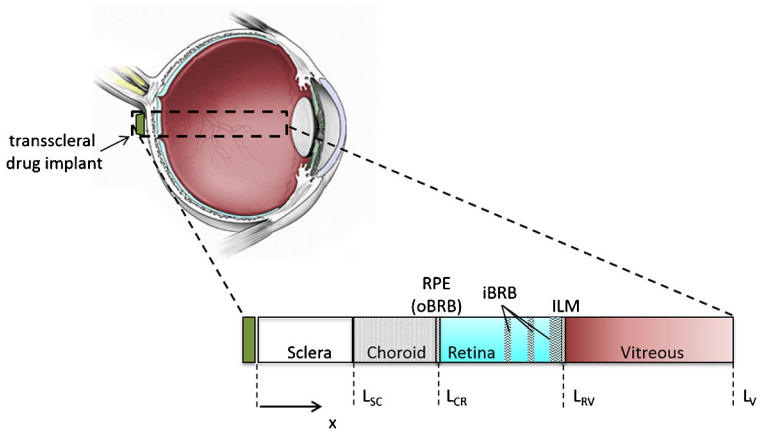

Figure 1 Globe of the eye and schematics of the PSE regions considered in the mathematical model. RPE: retinal pigmented epithelium, oBRB: outer blood retinal barrier, iBRB: internal blood retinal barrier, ILM: internal limiting membrane.

Figure 2 Schematic depiction of retinal circulation and corresponding mathematical model. Top: retinal tissue and circulation. Blood vessels are embedded in the inner retinal region, while the outer retina is avascular. The rightmost plexum is the arteriolar/venular network, middle and leftmost plexi are constitued by capillary networks. In the retinal tissue, different types of neural cells are represented. Bottom: mathematical representation of the function ϕ, volumetric fraction of blood in the multiphase model. The maximal values are attained in correspondance of the vessel plexi.

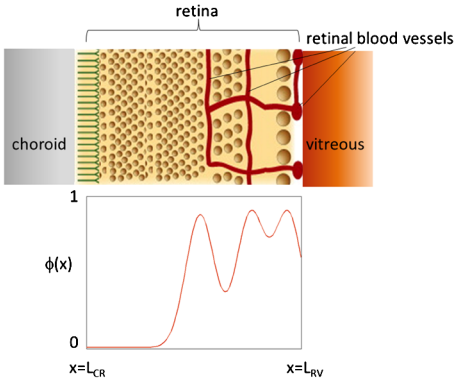

We denote by $\Omega_S = (0, L_{SC})$, $\Omega_C = (L_{SC}, L_{CR})$, $\Omega_R = (L_{CR}, L_{RV})$ and $\Omega_V = (L_{RV}, L_V)$ the computational domains corresponding to the S, C, R, V layers, respectively. For $j = S, C, R, V$, we denote by n_j its unit normal vector directed outward. For $i = S, C, R$ and $j = C, R, V$, we denote by Γ_{ij} the interface between two adjacent layers i and j.

2.2 Mathematical model of the PSE

Let $j = S, C, R, V$. For space $x \in \Omega_j$ and time $t \in (0, T)$, we let $v_j = v_j(x)$ (cm/s) be the steady filtration (seepage) velocity in layer j, $(K/\mu)_j$ the corresponding hydraulic conductivity (cm^2/mmHg/s). We let $C_j = C_j(t, x)$ (g/cm^3) be the drug concentration in layer j and D_j (cm^2/s) and k_j (1/s) the corresponding drug diffusivity and clearance/decay rate, respectively. For $i = S, C, R$ and $j = C, R, V$, we let $\mathcal{R}_{ij}$ (cm/s/mmHg) be the membrane hydraulic permeability at the interface Γ_{ij} and we let $\mathcal{L}_{ij}$ (cm/s) and $\mathcal{P}_{ij}$ $(\cdot)$ be the drug membrane permeability and the partition coefficient between the two layers.

Filtration velocity in the PSE. We model the interstitial flow as an incompressible fluid which permeates through the PSE porous layers according to the steady-state Darcy equation:

$$v_j = -\left(\frac{K}{\mu}\right)_j \frac{\partial p_j}{\partial x}, \tag{1}$$

$p_j = p_j(x)$ being the hydrostatic pressure. For $i = S, C, R$ and $j = C, R, V$, the following conditions hold at the interface Γ_{ij}:

- velocity continuity

$$v_i \cdot n_i = v_j \cdot n_i;$$

- pressure jump condition (reduced Kedem-Katchalsky conditions for solvent, see *e.g.*, [14])

$$v_i \cdot n_i = \mathcal{R}_{ij}(p_i - p_j).$$

Drug mass balance in the PSE. Drug mass balance is enforced in each layer according to the characteristic features of the layer itself.

In the *sclera* and *vitreous*, the following equation holds:

$$\frac{\partial C_j}{\partial t} = D_j \frac{\partial^2 C_j}{\partial x^2} - v_j \frac{\partial C_j}{\partial x} - k_j C_j, \quad j = S, V, \tag{2}$$

where v_j is computed from equation (1) in layer j.

Drugs in the *choroid* bloodstream rapidly equilibrate with the extravascular space, due to the fenestrated structure of choriocapillaris [15, 16]. For this reason, a unique concentration value is considered both for tissue and blood domains, yielding

$$\frac{\partial C_C}{\partial t} = S_C(t) + D_C \frac{\partial^2 C_C}{\partial x^2} - v_C \frac{\partial C_C}{\partial x} - k_C C_C, \tag{3}$$

where $S_C = S_C(t)$ is a systemic drug source rate, v_C is computed from equation (1) solved in the choroid and k_C the clearance rate due to choriocapillaries.

Drug concentration in the *retina* is modeled assuming the domain to contain a mixture of tissue and blood vessels. We denote by $\phi = \phi(x) \in (0,1)$ the retinal vascular porosity, which represents the volumetric fraction occupied by the vascular space, the remaining volumetric fraction being extravascular space. We have that $\phi \to 1$ in the inner regions where the vascular beds are located and $\phi \to 0$ in the outer regions. We consider a mathematical representation of the function ϕ as in Figure 2 (bottom panel) which results from the superposition of Gaussian functions centered in the anatomical location of each vessel plexum. The standard deviation of the Gaussian is chosen in such a way that the function is significantly greater than zero in a region roughly corresponding to the thickness of the vessel plexum itself (superficial layer and two capillary beds). We let $\beta = \beta(\phi)$ (1/s) be the rate of drug transport across the blood vessels representing the effect of the iBRB (see also [8, 17]). We set $\beta = \mathcal{L}_{vw} A_{\text{vessel}} \rho$, where $\mathcal{L}_{vw} \simeq 10^{-6}$ (cm/s) is the permeability of the blood vessel wall [18], $A_{\text{vessel}} \simeq 9 \cdot 10^{-6}$ (cm^2) the average lateral surface of a vessel (arteriole, capillary, venule [19]) and $\rho = \rho_{\max}\phi$ the number of vessels per cm^3 of tissue, with $\rho_{\max} \simeq 4.55 \cdot 10^6$ (1/cm^3) [15]. Denoting by $C_{Rt} = C_{Rt}(t,x)$ and $C_{Rb} = C_{Rb}(t,x)$ the drug concentration in tissue and vascular spaces, respectively, drug mass conservation is represented by the system:

$$\begin{cases} (1-\phi)\dfrac{\partial C_{Rt}}{\partial t} = (1-\phi)[D_R \dfrac{\partial^2 C_{Rt}}{\partial x^2} - (v_{Rt} + v_{act})\dfrac{\partial C_{Rt}}{\partial x} - k_{Rt} C_{Rt}] + \beta(C_{Rb} - C_{Rt}), \\ \phi \dfrac{dC_{Rb}}{dt} = S_{Rb}(t,x) - \beta(C_{Rb} - C_{Rt}) - \phi k_{Rb} C_{Rb}, \end{cases} \tag{4}$$

where $S_{Rb}(t,x) = \phi(x)\lambda(t)$ is a prescribed rate of drug concentration from systemic sources and v_{Rt} is computed from equation (1) solved in the retina. The additional filtration velocity v_{act}, pointing towards the negative x direction, is included in equation (4) to model active pumping by the RPE, which extracts fluid from the retina towards the choroid [8].

For $i = S, C, R$ and $j = C, R, V$, the following conditions for drug concentration are enforced at the interface Γ_{ij}:

- drug flux continuity

$$D_i \frac{\partial C_i}{\partial x} \cdot n_i = D_j \frac{\partial C_j}{\partial x} \cdot n_i;$$

- drug concentration jump condition (reduced Kedem-Katchalsky conditions for solute, see *e.g.*, [14])

$$-D_i \frac{\partial C_i}{\partial x} \cdot n_i = \mathcal{L}_{ij}(\mathcal{P}_{ij} C_i - C_j),$$

  where the partition coefficient $\mathcal{P}_{ij}$ takes into account the possible different hydrophilicity/lipophilicity between layers i and j.

The complete model for amounts to solve equation (1) along with equations (2)-(4) with the respective interface conditions. We enforce at the external boundary of the vitreous a hydrostatic pressure equal to 15 mmHg, corresponding to a normal intraocular pressure (IOP), and at the external boundary of the sclera a hydrostatic pressure equal to 10 mmHg, corresponding to the episcleral venous pressure [8]. For the drug, if not differently specified, we prescribe at the sclera external boundary a concentration exponentially decreasing in time from the initial value 1 mg/cm^3 fitting the trend obtained from a model of drug

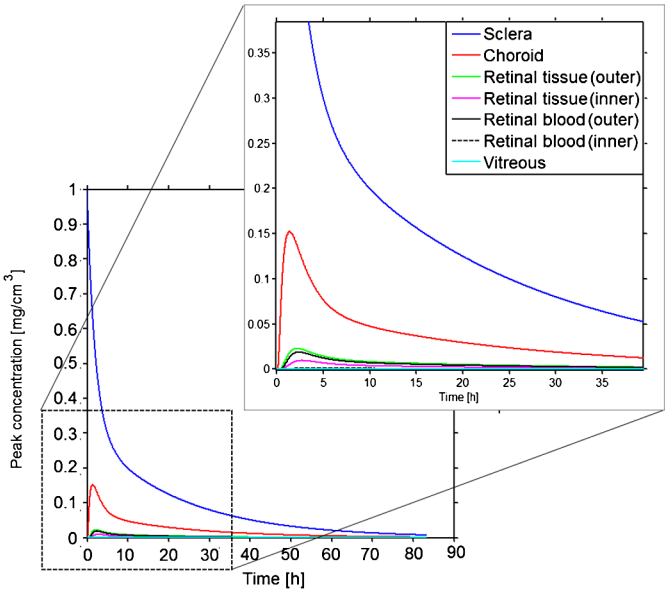

Figure 3 Drug peak concentration as a function of time in the different layers considered in the model. The curves relative to the retina are specified into tissue and blood phases and further divided into inner and outer region, the first indicating the portion of the retina embedding blood vessels (function $\phi > 1$) and the second one the avascular portion. The inset shows a zoom for short times.

release in posterior eye gel implants [17] (black curve in Figure 3 of the present paper). The vitreous is assumed to be thick enough so that there is no normal diffusive and convective flux of drug across its external boundary when considering episcleral drug delivery. The drug concentration problem is supplied by the initial conditions $C_j(t = 0, x) = C_{j,0}(x) = 0$, $j = S, C, R, V$ (exogenous drug).

3 Numerical simulations

The fluid filtration equations are solved numerically by means of the function `bvp4c` of MATLAB®. The drug concentration equations are solved using for time integration an explicit Runge-Kutta scheme with adaptive time step implemented by the function `ode23t` of MATLAB®. Spatial discretization is performed by an in-house developed code implementing 1D linear finite elements with stabilization techniques for possibly advection-dominated problems. The parameters used in the simulations are reported in Table 2. Notice that the external source terms S_C and S_{Rb} may be non-zero due to (a minimal) systemic drug absorption into circulation and successive release into the tissues. Being unable to quantify such sources, it is reasonable in first approximation to set $S_C = S_R = 0$.

3.1 Convective field

Solving the Darcy equations yields a constant filtration velocity of about 10^{-7} (cm/s). This value is in accordance with the results of [8, 20]. The corresponding Péclet number based on the layer thickness is definitely less than 1 when considering small weight molecules (diffusivity of the order of 10^{-7} to 10^{-6} (cm^2/s)) and of the order 1 when considering large

Table 2 Value of the model parameters used in the numerical simulations (if not specified otherwise)

Parameter	Value	Unit	Description	Ref.
t_S	600	μm	Sclera thickness	[13]
t_C	300	μm	Choroid thickness	[13]
t_R	246	μm	Retina thickness	[13]
t_V	15000	μm	Vitreous thickness	[20]
$(K/\mu)_S$	$8.4 \cdot 10^{-7}$	cm^2/s	Hydraulic conductivity in sclera	[8]
$(K/\mu)_C$	$2.35 \cdot 10^{-11}$	cm^2/s	Hydraulic conductivity in choroid	[8]
$(K/\mu)_R$	$1.5 \cdot 10^{-11}$	cm^2/s	Hydraulic conductivity in retina	[8]
$(K/\mu)_V$	1.5^{-11}	cm^2/s	Hydraulic conductivity in vitreous	[8]
$\mathcal{R}_{SC}$	10^{-7}	cm/s/mmHg	Hydraulic permeability at Γ_{SC}	[7, 32]
$\mathcal{R}_{CR}$	10^{-7}	cm/s/mmHg	Hydraulic permeability at Γ_{CR}	[7, 32]
$\mathcal{R}_{RV}$	10^{-7}	cm/s/mmHg	Hydraulic permeability at Γ_{RV}	[32]
D_S	$4 \cdot 10^{-7}$	cm^2/s	Drug diffusivity coefficient in sclera	[13]
D_C	$1.6 \cdot 10^{-7}$	cm^2/s	Drug diffusivity coefficient in choroid	[13]
D_R	$1.17 \cdot 10^{-7}$	cm^2/s	Drug diffusivity coefficient in retina	[13]
D_V	$6\ 10^{-6}$	cm^2/s	Drug diffusivity coefficient in vitreous	[6]
k_S	$3 \cdot 10^{-4}$	1/s	Drug clearance/Decay coefficient in sclera	[13]
k_C	$3 \cdot 10^{-4}$	1/s	Drug clearance/Decay coefficient in choroid	[13]
k_{Rt}	$3 \cdot 10^{-4}$	1/s	Drug clearance/Decay coefficient in retinal tissue	[13]
k_{Rb}	$3 \cdot 10^{-4}$	1/s	Drug clearance/Decay coefficient in retinal blood	[13]
k_V	$8 \cdot 10^{-5}$	1/s	Drug clearance/Decay coefficient in vitreous	[11]
$\mathcal{L}_{SC}$	10^{-4}	cm/s	Permeability coefficient at Γ_{SC}	[21]
$\mathcal{L}_{CR}$	10^{-5}	cm/s	Permeability coefficient at Γ_{CR}	[11, 16]
$\mathcal{L}_{RV}$	10^{-5}	cm/s	Permeability coefficient at Γ_{RV}	[11, 16, 21]
$\mathcal{P}_{CS}$	1	adim	Partition coefficient at sclera/Choroid interface	[21]
$\mathcal{P}_{CR}$	1/1.33	adim	Partition coefficient at choroid/Retina interface	[13]
$\mathcal{P}_{RV}$	1/10	adim	Partition coefficient at retina/Vitreous interface	[21]

weight molecules (diffusivity of the order of 10^{-8} (cm^2/s)). When considering in the retina the active pumping velocity, which is of the order of $8 \cdot 10^{-6}$ (cm/s) [8], the filtration velocity turns out to be negligible. The Péclet number of the retina computed with the pumping velocity rises to a value of the order of 20 for small molecules and 200 for large molecules, so that convection is dominating.

3.2 Validation of drug concentration levels

To validate the model, we check that we reproduce comparable results in drug peak concentration and time-to-peak as in existing literature models. In Figure 3, we show drug peak concentration as a function of time in the different layers considered in the model. The curves relative to the retina are specified into tissue and blood phases and further divided into inner and outer region, the first indicating the portion of the retina embedding blood vessels (function $\phi > 1$) and the second one the avascular portion In Figures 4 and 5, we report results from simulations in different literature models for molecules comparable to fluoroscein and for similar drug inlet boundary conditions with episcleral plug or injection. The peak concentration value found in our simulations is comparable to the one of the models of [17] and [13] (scaled inlet concentration) in the retina and to the ones of the models of [8] and [13] (scaled inlet concentration) in the choroid. Time-to peak values

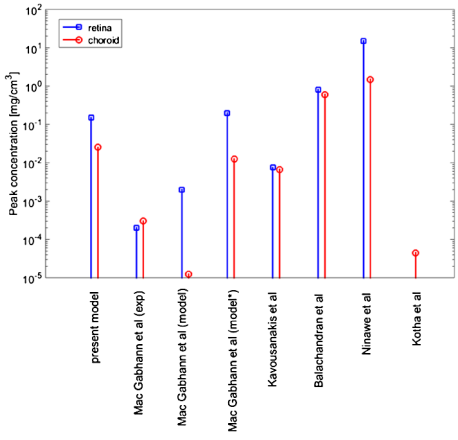

Figure 4 Drug peak concentration values for the present model and literature models (data represented are where available and upon conversion of units of measure). Comparable values of parameters and inlet conditions are used. Values denoted by the symbol '$*$' have been obtained by multiplying the values by 100 to scale drug concentration at the boundary (assuming a linear behavior as suggested by the results of [21]). Values from [8] have been interpreted as percentage of the enforced boundary concentration, in lack of indications. Notice that log scale is used for the *y* axis.

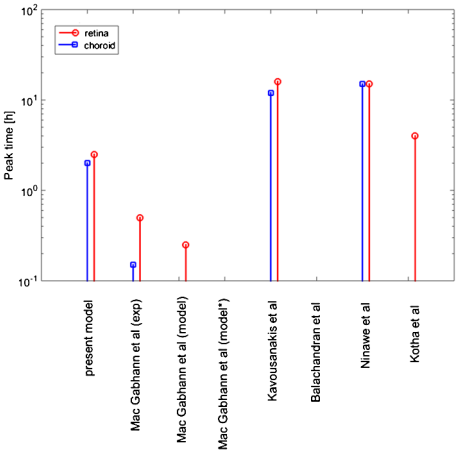

Figure 5 Drug time-to-peak values for the present model and literature models (data are represented where available and upon conversion of units of measure). Comparable values of parameters and inlet conditions are used. Notice that log scale is used for the *y* axis.

of our model, of the order of 1-2 (h), comparable to the results of [21]. Such a scattering of the results may be ascribed to (i) different dimensionality of the models; (ii) different values of the parameters (see the below sensitivity study); (iii) different biophysical mechanisms included (active pumping, filtration velocity, membrane permeabilities, membrane partition coefficient). The following sensitivity analysis is aimed at clarifying the role of the different parameters and mechanisms.

3.3 Sensitivity study

We use now the model to study the sensitivity of the drug peak concentration and drug time-to-peak with respect to: (i) diffusion coefficients; (ii) clearance rates; (iii) membrane permeabilities; (iv) convective velocity. Values of the parameters reported in Table 2 are considered as the baseline condition. The filtration velocity is artificially varied as a synthetic index of the variation of hydraulic permeability and pressure drop and the boundaries. We vary each parameter individually and we plot for the retina and choroid the resulting peak concentration (Figure 6) and time-to-peak (Figure 7) as a function of the parameter value. The different colored lines represent peak concentration or time-to-peak when the parameter in object is changed in a certain layer (refer to the legend in each panel). Vertical dotted lines in each panel show the parameter baseline value.

In Figure 8, we show the drug peak concentration as a function of time with active or inactive selected components of the convective field in baseline conditions. In Figure 9 we show the sensitivity of the drug peak concentration and time-to-peak values in tissue and blood phases of the retina. with respect to the different components of the convective field (filtration velocity and active pumping). The choroid (data not reported) results to be very weakly sensitive to the variations in the convective field values.

4 Discussion and conclusions

Drug delivery to the PSE is still an open issue in ocular diseases therapy. Many drugs have a narrow concentration window within which they are effective and non-toxic. Currently, about 90% of the treatments of ophthalmic diseases are performed by medications administered topically. However, drugs enter the eye through this pathway at a very limited extent: wash off by various mechanisms (lacrimation, blinking, tear turnover) and low permeability of the corneal epithelial membrane causes less than 5% of the administered drug to effectively reach the posterior targets [22]. Among the other possible drug delivery routes, systemic administration has a poor dose/response profile in the eye. Intravitreous delivery, whilst efficient, can carry significant local complications such as retinal detachment, endophthalmitis, vitreous hemorrhage and cataract formation [23]. Under these premises, sustained drug delivery to the PSE via the alternative transscleral route is gaining increasing importance, due to the easily accessible area, the hypocellularity and permeability of the sclera to relatively large molecules, and, importantly, to the degree of acceptance of patients [24, 25]. Pharmacokinetics of drugs in the PSE following transscleral delivery is an emerging issue [4]. The reported data are very sparse and, for the most part, refer only to the vitreous, which is easily accessible in experiments, to draw comparisons.

Transscleral drug delivery has been analyzed in this paper using a 1D continuum model including diffusive, convective and reactive mechanisms and comprehending the sclera, choroid, retina and vitreous domains. The presence of internal membranes has been kept

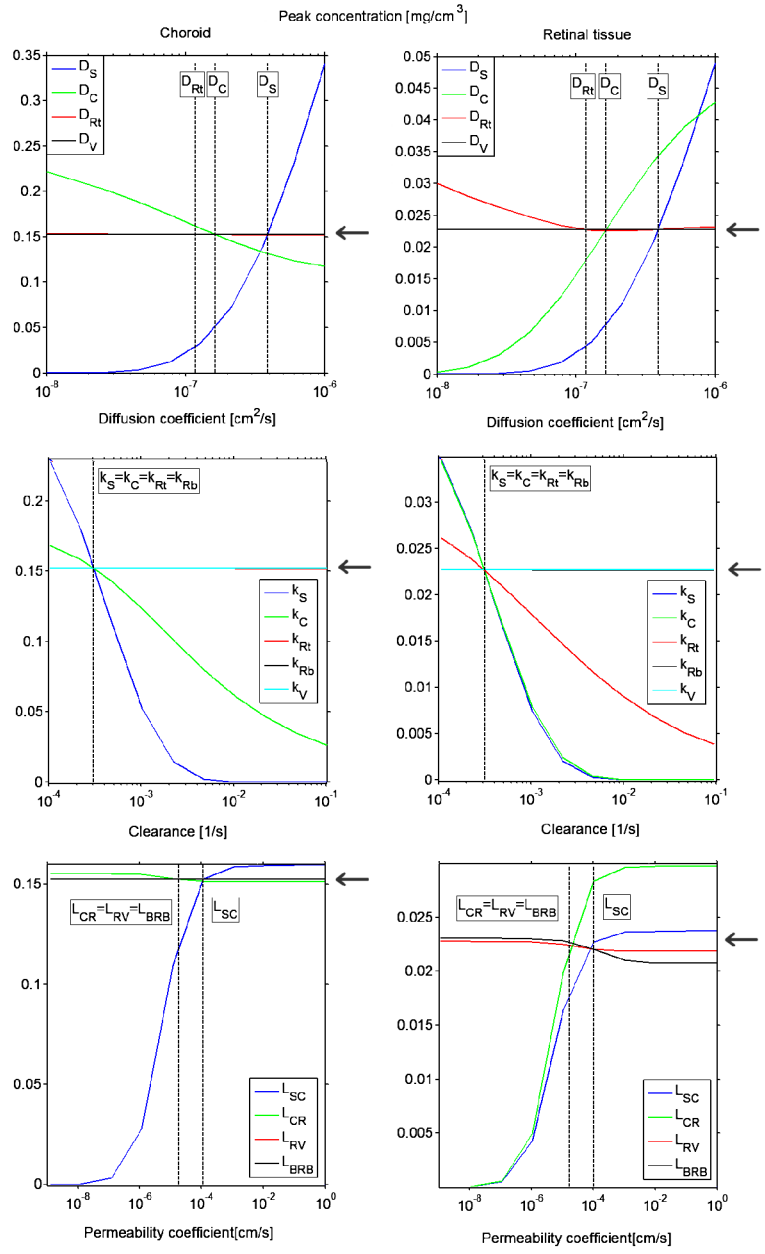

Figure 6 Drug peak concentration in the choroid (left column) and retina (right column) as a function of diffusion coefficient (top row), clearance rate (middle row) and membrane permeability (bottom row) in the various layers (specified in the legends). The dotted vertical lines indicate baseline values of the parameters. Arrows indicate the value of concentration in baseline conditions.

into account by appropriate interface boundary conditions and/or a fictitious advective field for RPE active pumping. Drug concentration levels in the retina have been modeled distinguishing the tissue phase from the blood phase.

In [13], the partial failure in reproducing with the mathematical model the experimental results is ascribed to the discrepancy of the values of the parameters estimated from basic physical considerations vs values of the parameters obtained by fitting the model to experimental data. This fact suggested to explore ranges of parameter values to identify

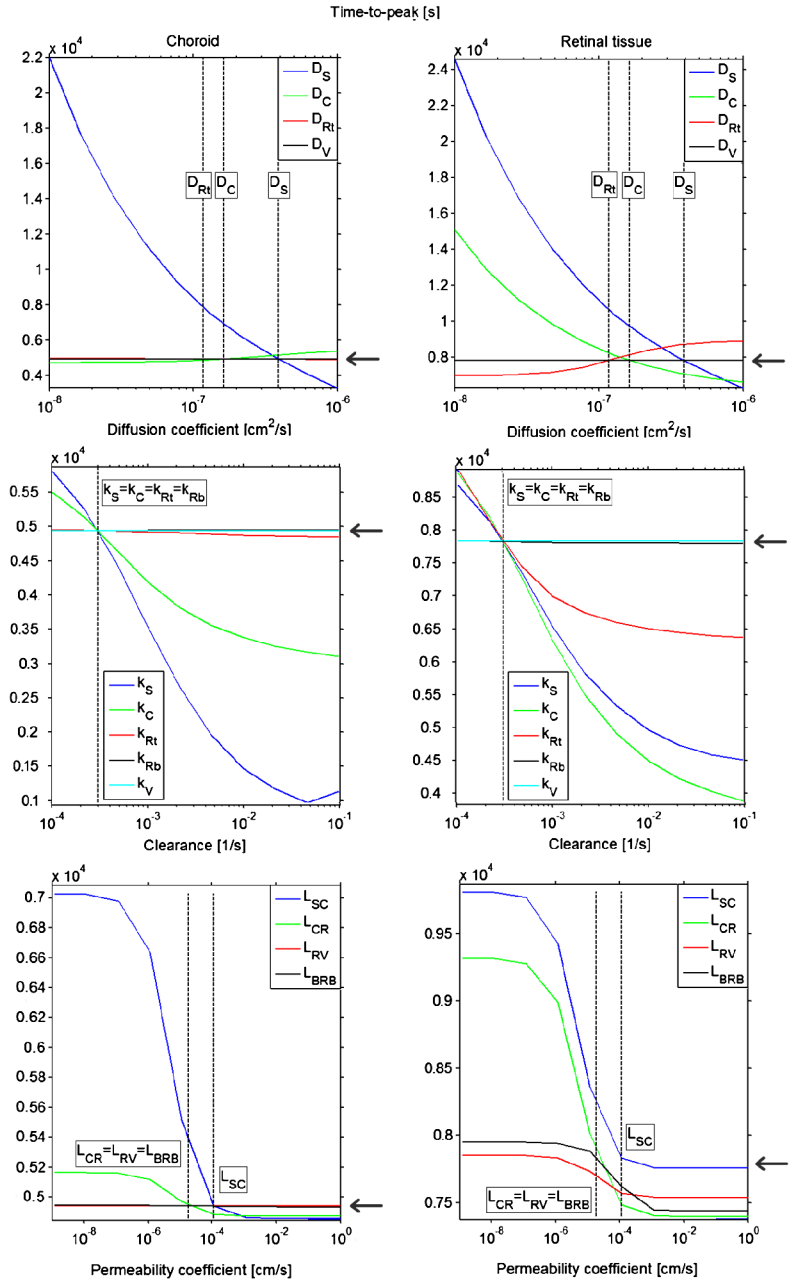

Figure 7 Drug time-to-peak in the choroid (left column) and retina (right column) as a function of diffusion coefficient (top row), clearance rate (middle row) and membrane permeability (bottom row) in the various layers (specified in the legends). The dotted vertical lines indicate baseline values of the parameters. Arrows indicate the value of time-to-peak in baseline conditions.

characteristic model sensitivities. The authors found a relatively low sensitivity of peak concentration and time-to-peak in the retina to the diffusion and clearance coefficients and a higher sensitivity to drug resistance (inverse of the drug permeability) of the episcleral layers with respect to peak concentration and to RPE resistance. However, while it is clearly recognized that a major fraction of the drug is lost from episcleral lymphatics and blood vessels [11], one can think to eliminate the exceedingly large influence of such a

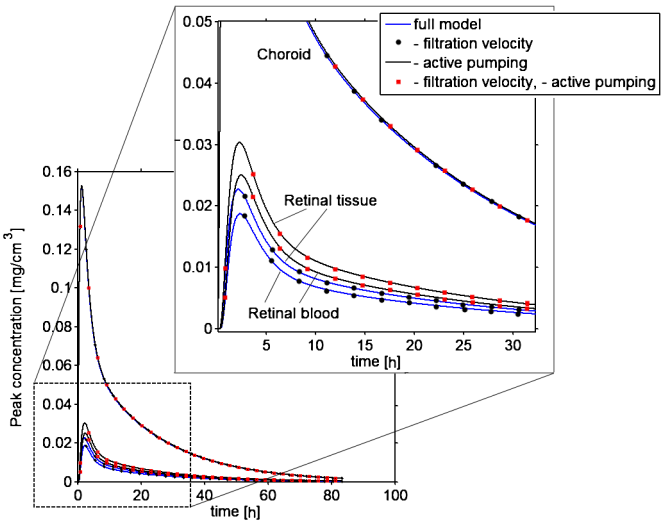

Figure 8 Drug peak concentration and time-to-peak as a function of time with active or inactive ('-') selected components of the convective field in baseline conditions.

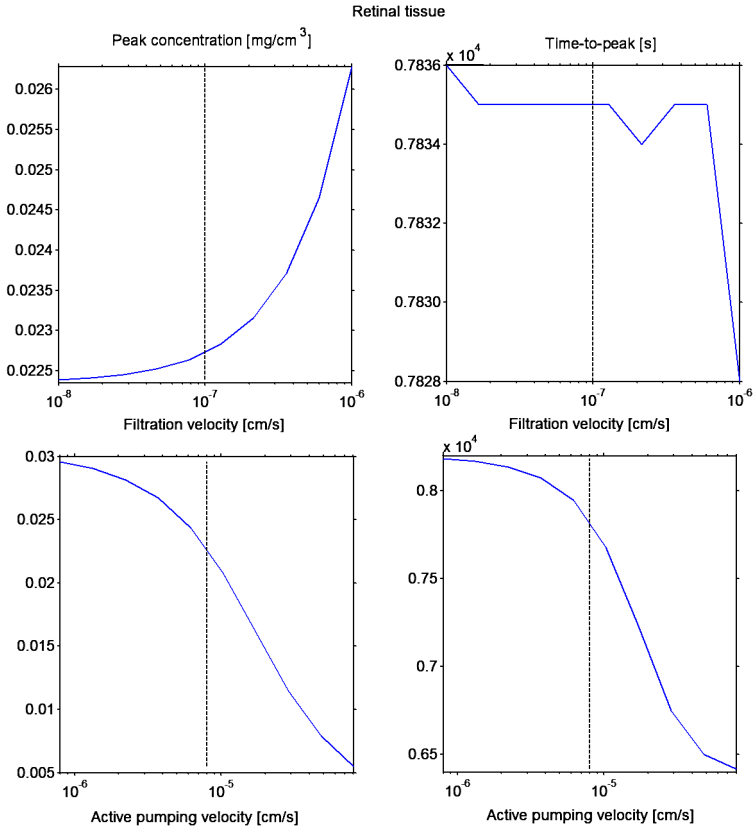

Figure 9 Sensitivity study of the drug peak concentration and time-to-peak values in tissue and blood phases of the retina with respect to the different components of the convective field (filtration velocity, top row and active pumping, bottom row). The choroid (data not reported) results to be very weakly sensitive to variations of the convective field values.

mechanism and just focus on the area from sclera to vitreous. Varying the parameters in the same range as in [13] yields in this work sensitivities which reflect comparable, if not more important, roles of diffusion and clearance rates.

As for the convective field, it is apparent that the filtration velocity is too low to induce significant changes (see Figure 8). Different is the case of the active pumping velocity. Accordingly to what found in [8] and [21] (notice that in these references, the authors represent this same mechanism in a different way), active pumping plays a very relevant role, if one looks specifically at the retina and possibly at the vitreous. It is interesting to observe the shape of the curves with respect to drug permeability. Both for peak concentration and time-to-peak, the curves results relatively flat even varying the parameter of 1 or 2 decades in log scale. This is probably due to permeability not being a limiting phenomenon in these regions. The iBRB drug permeability does not seem to have a major role except for a region of diameter spanning about 1 decade at the left and at the right of the baseline value, where the slope of the curve is comparable to the other ones. The mild influence of iBRB might due to having neglected the complexity of active/carried-mediated transport mechanisms across these interfaces and having considered a single partition coefficient across the vessel walls in both (inward and outward) directions. Representing active pumping as a fictitious velocity and not as a membrane effect, hinders the role of RPE (see [21] for this choice).

An important result of the present analysis is the way in which a 30% increase of the drug peak concentration in choroid and retina can be obtained from the baseline values, for example to meet a therapeutic threshold. Assuming continuous dependence of the solution on data - a property which can be inferred via a mathematical analysis not much different to the one performed in the Appendix - it is found that such an increase can be obtained acting on (i) scleral biophysical parameters and then on choroidal and retinal ones; (ii) active pumping. As for (i), in the neighborhood of baseline conditions, diffusion and clearance appear to play a comparable role, because comparable variations in the scleral diffusion (increase) or scleral clearance (decrease) are required to increase drug peak concentration (notice the slope of the curves in Figure 6). The sclera is permeable to hydrophilic compounds, even macromolecules, but the permeability in the RPE/choroid/Bruch's membrane is 1-2 orders of magnitude lower than in the sclera [16]. Moreover, the trend line of decreasing choroid-Bruch's membrane permeability with increasing solute lipophilicity and/or molecular radius appears to be steeper than the sclera. However, the simulations suggest that the slope of the sensitivity curves is always higher for the scleral parameters that for the choroidal ones. Moreover, sensitivity in a certain layer is higher to properties of layers located at its left side than at its right side. This is a natural consequence of the positioning of the source. In particular, referring to the theoretical analysis carried out for the retinal domain, this implies that the drug concentration in the choroid is always responsible for the upper bound. As for (ii), pro-drugs have been envisaged as carriers able to favorably enhance drug delivery. This a very advanced issue in pharmacokinetics, we refer to [26] for a general review.

The present model does not allow to provide data regarding the 3D spatial distribution of the drug on the eye globe. While this aspect is very important and has been recently considered in a few mathematical models [8, 17, 21], it remains very difficult to compare results from such models with experiments. Unknown boundary conditions in the 3D models, on the one hand, and tissue homogenization after explant with loss of spatial dependence, on the other, are just examples of such problems.

Appendix: Bounds for drug concentration in the retina

The retina is an important target for therapies to contrast several disorders, including diabetic retinopathy, age-related macular degeneration, and retinitis pigmentosa [27]. The retina has a unique position with regard to pharmacokinetics, being separated from circulating blood by the BRBs, makes it a very difficult target. In this section, we theoretically establish the bounds for drug concentration predicted by the model in the retinal domain Ω_R, assuming for simplicity no convective field. To do this, we assume the drug concentration at the interface with the adjacent choroid ($\bar{C}_C = \bar{C}_C(t)$) and vitreous ($\bar{C}_V = \bar{C}_V(t)$) to be known functions, so that the boundary conditions for the domain Ω_R become:

$$-D_{Rt}\frac{\partial C_{Rt}}{\partial x}\cdot n_{Rt} = \mathcal{L}_{CR}(\mathcal{P}_{CR}C_{Rt} - \bar{C}_C) \quad \text{on } \Gamma_{CR}, \tag{5}$$

$$-D_{Rt}\frac{\partial C_{Rt}}{\partial x}\cdot n_{Rt} = \mathcal{L}_{RV}(\mathcal{P}_{RV}C_{Rt} - \bar{C}_V) \quad \text{on } \Gamma_{RV}. \tag{6}$$

In the sequel, $L^2(\Omega_R)$ will denote the space of measurable functions whose square is Lebesgue integrable in Ω_R. The space $L^2(\Omega_R)$ is equipped with the norm $\|\cdot\|_{L^2(\Omega_R)}$. We denote with $(\cdot,\cdot)$ its scalar product both for scalar and vector functions. We introduce the Sobolev space $H^1(\Omega_R)$, which denotes functions that belong to $L^2(\Omega_R)$ along with their first order distributional derivative in space. For $v \in H^1(\Omega_R)$, we denote by $\partial_x v$ such a derivative. The space $H^1(\Omega_R)$ is equipped with the norm $\|\cdot\|_{H^1(\Omega_R)}$. We also need to introduce the spaces $L^2(0,T;V) = \{v : (0,T) \to V | v(t) \text{ is measurable}, \|v\|^2_{L^2(0,T;V)} := \int_0^T \|v(t)\|_V^2\, dt < +\infty\}$, with $V = H^1(\Omega_R)$ or $L^2(\Omega_R)$, and $L^\infty(0,T;L^2(\Omega_R)) = \{v : (0,T) \to L^2(\Omega_R) | v(t) \text{ is measurable}, \|v(t)\|^2_{L^2(\Omega_R)} \text{ is essentially bounded in } (0,T)\}$, endowed with the norm $\|v\|_{L^\infty(0,T;L^2(\Omega_R))} := \inf\{M > 0 : \|v(t)\|^2_{L^2(\Omega_R)} \le M \text{ a.e. in } (0,T)\}$. For $v \in L^2(0,T;V)$, we denote by $\partial_t v$ its derivative with respect to time, such that $\partial_t v \in L^2(0,T;V'(\Omega_R))$, V' being the dual space of V, and $\forall u \in L^2(0,T;V)$, $\langle \partial_t v(t), u(t)\rangle = \int_{\Omega_R} \partial_t v u\, dx$ represents a duality pairing. We here assume for simplicity that D_R, k_{Rt}, k_{Rb}, $\mathcal{L}_{CR}$, $\mathcal{L}_{RV}$ are positive constants and that $\beta \in L^\infty(\Omega_R)$ and $C_{Rb,0}, C_{Rt,0} \in L^2(\Omega_R)$. We let $\phi \in C^0(\bar{\Omega}_R)$ with $\phi_m = \min_{x\in\Omega_R}\phi(x)$ and $\phi_M = \max_{x\in\Omega_R}\phi(x)$.

The weak counterpart of the multiphase system (4) reads:

- in the tissue phase, find $C_{Rt} = C_{Rt}(t,x) \in L^2(0,T;H^1(\Omega_R))$ with $\partial_t C_{Rt} \in L^2(0,T;H^{-1}(\Omega_R))$, such that:

$$\begin{aligned}\big\langle(1-\phi)\partial_t C_{Rt}, v\big\rangle + D_R\big((1-\phi)\partial_x C_{Rt}, \partial_x v\big) + \big(k_R(1-\phi)C_{Rt}, v\big)\\ + \big(\beta(C_{Rt} - C_{Rb}), v\big) + \mathcal{L}_{CR}\big((1-\phi)(C_{Rt} - \mathcal{P}_{CR}\bar{C}_C), v\big)|_{\Gamma_{CR}}\\ + \mathcal{L}_{RV}\big((1-\phi)(\mathcal{P}_{RV}C_{Rt} - \bar{C}_V)v\big)|_{\Gamma_{RV}} = 0 \quad \forall v \in H^1(\Omega_R);\end{aligned} \tag{7}$$

- in the blood phase, find $C_{Rb} = C_{Rb}(t,x) \in L^2(0,T;L^2(\Omega_R))$ with $\partial_t C_{Rb} \in L^2(0,T;L^2(\Omega_R))$, such that:

$$\langle\phi\partial_t C_{Rb}, w\rangle + (k_{Rb}\phi C_{Rb}, w) + \big(\beta(C_{Rb} - C_{Rt}), w\big) = (S_{Rb}, w) \quad \forall w \in L^2(\Omega_R). \tag{8}$$

We prove that the drug concentration in the multiphase model is non-negative and bounded above by a maximal value C_N depending on the initial conditions, boundary data and external sources. In doing this, we neglect the convective field.

Theorem 1 *Let* $C_N := \max\{\max_{t\in(0,T)}\{\mathcal{P}_{CR}\bar{C}_C, \frac{\bar{C}_V}{\mathcal{P}_{RV}}, \frac{\lambda(t)}{k_{Rb}}\}, \max_{x\in\Omega_R}\{C_{Rb,0}, C_{Rt,0}\}\}$. *Then, the solution* $C_R = C_R(t,x) = [C_{Rt}(t,x), C_{Rb}(t,x)]$ *of problem* (7)-(8) *satisfies* $0 \le C_R(t,x) \le C_N$ *a.e. in* $\Omega_R \times (0,T)$.

Proof of Theorem 1 We face the multiphase problem in the retina in a decoupled manner by introducing the following Gauss-Seidel iterative procedure:

Given $0 \le C^0_{Rb} \le C_N$ a.e. in $\Omega_R \times (0,T)$, $\forall k = 1,2,\dots$, find $C^k_R = [C^k_{Rt}, C^k_{Rb}] \in L^2(0,T; H^1(\Omega_R)) \times L^2(0,T; L^2(\Omega_R))$ such that it yields:

- in the tissue phase

$$\begin{aligned}&\langle(1-\phi)\partial_t C^k_{Rt}, v\rangle + D_R\big((1-\phi)\partial_x C^k_{Rt}, \partial_x v\big) + \big(k_R(1-\phi)C^k_{Rt}, v\big)\\ &\quad + \big(\beta\big(C^k_{Rt} - C^{k-1}_{Rb}\big), v\big) + \mathcal{L}_{CR}\big((1-\phi)\big(C^k_{Rt} - \mathcal{P}_{CR}\bar{C}_C\big), v\big)|_{\Gamma_{CR}}\\ &\quad + \mathcal{L}_{RV}\big((1-\phi)\big(\mathcal{P}_{RV}C^k_{Rt} - \bar{C}_V\big)v\big)|_{\Gamma_{RV}} = 0 \quad \forall v \in H^1(\Omega_R);\end{aligned} \tag{9}$$

- in the blood phase

$$\langle\phi\partial_t C^k_{Rb}, w\rangle + \big(k_{Rb}\phi C^k_{Rb}, w\big) + \big(\beta\big(C^k_{Rb} - C^k_{Rt}\big), w\big) = (S_{Rb}, w) \quad \forall w \in L^2(\Omega_R). \tag{10}$$

We verify by a recursive argument that the sequence C^k_R satisfies $0 \le C^k_R \le C_N$. The key point is given by the following lemma, for $k = 1,2,\dots$.

Lemma 1 *Given* $0 \le C^{k-1}_{Rb} \le C_N$ *in* $\Omega_R \times (0,T)$, *then* $0 \le C^k_{Rt} \le C_N$ *in* $\Omega_R \times (0,T)$. *Conversely, given* $0 \le C^k_{Rt} \le C_N$ *in* $\Omega_R \times (0,T)$, *then* $0 \le C^k_{Rb} \le C_N$ *in* $\Omega_R \times (0,T)$.

Proof of Lemma 1 Let ℓ be a constant. For any $u \in V$, we introduce the non-negative functions $[u-\ell]^+ = \max\{u-\ell, 0\}$, $[u-\ell]^- = \max\{\ell - u, 0\}$, such that $[u-\ell]^+, [u-\ell]^- \in V$. We refer to [28] for the properties of such functions.

We start proving that $C^k_R \ge 0$ under the hypothesis that $C^{k-1}_{Rb} \ge 0$. We set $\ell = 0$ and choose $v = -[C_{Rt}]^-$ as a test function in (9), yielding

$$\begin{aligned}&\frac{1}{2}(1-\phi_M)\frac{d}{dt}\big\|\big[C^k_{Rt}\big]^-\big\|^2_{L^2(\Omega_R)} + D_R(1-\phi_M)\big\|\partial_x\big[C^k_{Rt}\big]^-\big\|^2_{L^2(\Omega_R)}\\ &\quad + \big(k_R(1-\phi_M) + \beta(\phi_m)\big)\big\|\big[C^k_{Rt}\big]^-\big\|^2_{L^2(\Omega_R)}\\ &\quad + \mathcal{L}_{RV}\mathcal{P}_{RV}\big((1-\phi)\big(\big[C^k_{Rt}\big]^-\big)^2\big)_{|\Gamma_{RV}} + \mathcal{L}_{CR}\big((1-\phi)\big(\big[C^k_{Rt}\big]^-\big)^2\big)_{|\Gamma_{CR}}\\ &\le -\beta(\phi_m)\int_{\Omega_R} C^{k-1}_{Rb}\big[C^k_{Rt}\big]^- dx - \mathcal{L}_{CR}\mathcal{P}_{CR}\bar{C}_C\big((1-\phi)\big[C^k_{Rt}\big]^-\big)_{|\Gamma_{CR}}\\ &\quad - \mathcal{L}_{RV}\bar{C}_V\big((1-\phi)\big[C^k_{Rt}\big]^-\big)_{|\Gamma_{RV}}.\end{aligned} \tag{11}$$

The right-hand of side of (11) is non-positive for a.e. $t \in (0,T)$. Integrating in time over $(0,t)$ and using the fact that $[C^k_{Rt,0}]^- = 0$, we obtain

$$\begin{aligned}&\big\|\big[C^k_{Rt}(t)\big]^-\big\|^2_{L^2(\Omega_R)} + 2D_R\int_0^t\big\|\partial_x\big[C^k_{Rt}\big]^-\big\|^2_{L^2(\Omega_R)} + 2\left(k_R + \frac{\beta(\phi_m)}{1-\phi_M}\right)\int_0^t\big\|\big[C^k_{Rt}\big]^-\big\|^2_{L^2(\Omega_R)}\\ &\quad + 2\mathcal{L}_{RV}\mathcal{P}_{RV}\int_0^t\big(\big[C^k_{Rt}\big]^-\big)^2_{|\Gamma_{RV}} + 2\mathcal{L}_{CR}\int_0^t\big(\big[C^k_{Rt}\big]^-\big)^2_{|\Gamma_{CR}} \le 0.\end{aligned} \tag{12}$$

We evaluate the integrals at the left-hand side of (12) for $t = T$ and integrate once again, this time on $[0, T]$, obtaining:

$$\begin{aligned}&\min\left\{1 + 2T\left(k_R + \frac{\beta(\phi_m)}{1-\phi_M}\right), 2D_R T\right\} \left\| \left[C_{Rt}^k\right]^- \right\|^2_{L^2(0,T;H^1(\Omega_R))} \\ &\quad + 2T\mathcal{L}_{RV}\mathcal{P}_{RV} \int_0^T \left(\left[C_{Rt}^k\right]^-_{|\Gamma_{RV}}\right)^2 + 2T\mathcal{L}_{CR} \int_0^T \left(\left[C_{Rt}^k\right]^-_{|\Gamma_{CR}}\right)^2 \leq 0. \end{aligned} \tag{13}$$

From (13) we deduce that $[C_{Rt}^k(t)]^- = 0$ and thus $C_{Rt}^k \geq 0$ a.e. in $\Omega_R \times (0, T)$. Now, we choose $v = -[C_{Rb}]^-$ as a test function in (10), yielding

$$\begin{aligned}&\frac{1}{2}\phi_m \frac{d}{dt} \left\| \left[C_{Rb}^k\right]^- \right\|^2_{L^2(\Omega_R)} + \left(\beta(\phi_m) + \phi_m k_{Rb}\right) \left\| \left[C_{Rb}^k\right]^- \right\|^2_{L^2(\Omega_R)} \\ &\quad \leq -\beta(\phi_m) \int_{\Omega_R} \left(C_{Rt}^k\right)\left[C_{Rb}^k\right]^- dx - \int_{\Omega_R} S_{Rb}(t, \phi_m)\left[C_{Rb}^k\right]^- dx. \end{aligned} \tag{14}$$

Thanks to the previous result and to the hypotheses on the external source, the right-hand of side of (14) is non-positive for a.e. $t \in (0, T)$. Integrating in time over $(0, t)$ and using the fact that $[C_{Rt,0}^k]^- = 0$, we obtain:

$$\begin{aligned}&\left\| \left[C_{Rb}^k(t)\right]^- \right\|^2_{L^2(\Omega_R)} + 2\left(\frac{\beta(\phi_m)}{\phi_m} + k_{Rb}\right) \int_0^t \left\| \left[C_{Rb}^k\right]^- \right\|^2_{L^2(\Omega_R)} \\ &\quad \leq -2\frac{\beta(\phi_m)}{\phi_m} \int_0^t \int_{\Omega_R} \left(C_{Rt}^k\right)\left[C_{Rb}^k\right]^- dx - 2\int_0^t \int_{\Omega_R} \frac{S_{Rb}(t, \phi_m)}{\phi_m}\left[C_{Rb}^k\right]^- dx. \end{aligned} \tag{15}$$

We evaluate the integrals at the left-hand side for $t = T$ and integrate once again, this time on $[0, T]$, obtaining:

$$\left(1 + 2T\left(\frac{\beta(\phi_m)}{\phi_m} + k_{Rb}\right)\right) \left\| \left[C_{Rb}^k\right]^- \right\|^2_{L^2(0,T;L^2(\Omega_R))} \leq 0. \tag{16}$$

From (16) we deduce that $[C_{Rb}^k(t)]^- = 0$ and thus $C_{Rb}^k \geq 0$ a.e. in $\Omega_R \times (0, T)$.

Now we prove that $C_R^k \leq C_N$ under the hypothesis $C_{Rb}^{k-1} \leq C_N$. We set $\ell = C_N$ and we choose $v = [C_{Rt}^k - C_N]^+$ as a test function in (9), yielding

$$\begin{aligned}&\min\left\{1 + 2T\left(k_R + \frac{\beta(\phi_m)}{1-\phi_M}\right), 2D_R T\right\} \left\| \left[C_{Rt}^k - C_N\right]^+ \right\|^2_{L^2(0,T;H^1(\Omega_R))} \\ &\quad + C_N k_R T \int_0^T \int_{\Omega_R} \left[C_{Rt}^k - C_N\right]^+ dx\, dt \\ &\quad + \frac{\beta(\phi_m)}{1-\phi_M} T \int_0^T \int_{\Omega_R} \left[C_{Rt}^k - C_N\right]^+ \left(C_N - C_{Rb}^{k-1}\right) dx\, dt \\ &\quad + \mathcal{L}_{RV}\mathcal{P}_{RV} T \int_0^T \left(\left[C_{Rt}^k - C_N\right]^+\right)^2_{|\Gamma_{RV}} dt + \mathcal{L}_{CR} T \int_0^T \left(\left[C_{Rt}^k - C_N\right]^+\right)^2_{|\Gamma_{CR}} dt \\ &\quad + \mathcal{L}_{RV}(\mathcal{P}_{RV} C_N - \bar{C}_V) T \int_0^T \left[C_{Rt}^k - C_N\right]^+_{|\Gamma_{RV}} dt \\ &\quad + \mathcal{L}_{CR} T \int_0^T (C_N - \mathcal{P}_{CR}\bar{C}_C)\left[C_{Rt}^k - C_N\right]^+_{|\Gamma_{CR}} dt \leq 0. \end{aligned} \tag{17}$$

Proceeding in a similar way as above, we deduce that $\|[C_{Rt}^k - C_N]^+\|^2_{L^2(0,T;H^1(\Omega_R))} = 0$, which directly implies that $C_{Rt}^k \le C_N$ a.e. in $\Omega_R \times (0,T)$. Now, we choose $\nu = [C_{Rb}^k - C_N]^+$ as a test function in (10), yielding

$$\begin{aligned}
&\phi_m \frac{1}{2}\frac{d}{dt}\left\|\left[C_{Rb}^k - C_N\right]^+\right\|^2_{L^2(\Omega_R)} + \left(\phi_m k_{Rb} + \beta(\phi_m)\right)\left\|\left[C_{Rb}^k - C_N\right]^+\right\|^2_{L^2(\Omega_R)} \\
&\quad \le -\beta(\phi_m)\int_{\Omega_R}\left(C_N - C_{Rt}^k\right)\left[C_{Rb}^k - C_N\right]^+ dx \\
&\qquad - \int_{\Omega_R}\left(\phi\left(k_{Rb}C_N - \lambda(t)\right)\right)\left[C_{Rb}^k - C_N\right]^+ dx. \qquad (18)
\end{aligned}$$

Upon observing that all the terms at the right and side are non-positive, we integrate in time over $(0,T)$ using the fact that $[C_{Rb,0}^k - C_N]^+ = 0$ and we integrate once again on $[0,T]$, obtaining

$$\left(\phi_m + 2T\left(\beta(\phi_m) + \phi_m k_{Rb}\right)\right)\left\|\left[C_{Rb}^k - C_N\right]^+\right\|^2_{L^2(0,T;L^2(\Omega_R))} \le 0.$$

We deduce that $\|[C_{Rb}^k - C_N]^+\|^2_{L^2(0,T;L^2(\Omega_R))} = 0$, that directly implies that $C_{Rb}^k \le C_N$ a.e. in $\Omega_R \times (0,T)$. □

To conclude the theorem, we prove the following lemma.

Lemma 2 *The sequence C_R^k converges to the solution of system* (7)-(8), *precisely*

$$\begin{aligned}
&\lim_{k\to\infty}\left\|C_{Rt} - C_{Rt}^k\right\|_{L^2(0,T;H^1(\Omega_R))} = 0, \\
&\lim_{k\to\infty}\left\|C_{Rb} - C_{Rb}^k\right\|_{L^2(0,T;L^2(\Omega_R))} = 0, \\
&\lim_{k\to\infty}\left\|C_R - C_R^k\right\|_{L^\infty(0,T;[L^2(\Omega_R)]^2)} = 0.
\end{aligned}$$

Proof of Lemma 2 We introduce the splitting errors $e_{Rt}^k := C_{Rt} - C_{Rt}^k$, $e_{Rb}^k := C_{Rb} - C_{Rb}^k$. We observe that $e_{Rt}^k \in H^1(\Omega_R)$ and $e_{Rb}^k \in L^2(\Omega_R)$. We subtract the corresponding equations of (7)-(8) from equations (9)-(10), and we choose as tests functions e_{Rt}^k and e_{Rb}^k in the first and second system, respectively. Then we integrate each equation over $(0,T)$ and sum up the two inequalities, term by term. Noticing that $e_{Rt}^k = e_{Rb}^k = 0$ at time $t = 0$ for all k and considering the summation over k from 0 to a given index M, we have at time T,

$$\begin{aligned}
&\sum_{k=1}^{M}\Bigg((1-\phi_M)\left\|e_{Rt}^k\right\|^2_{L^2(\Omega_R)} + \phi_m\left\|e_{Rb}^k\right\|^2_{L^2(\Omega_R)} + 2(1-\phi_M)D_R\int_0^T\left\|\partial_x e_{Rt}^k\right\|^2_{L^2(\Omega_R)}dt \\
&\qquad + 2(1-\phi_M)k_{Rt}\int_0^T\left\|e_{Rt}^k\right\|^2_{L^2(\Omega_R)}dt + 2\phi_m k_{Rb}\int_0^T\left\|e_{Rb}^k\right\|^2_{L^2(\Omega_R)}dt \\
&\qquad + 2(1-\phi_M)\mathcal{L}_{RV}\mathcal{P}_{RV}\int_0^T\left(e_{Rt}^k\right)^2_{|\Gamma_{RV}}dt + 2(1-\phi_M)\mathcal{L}_{CR}\int_0^T\left(e_{Rt}^k\right)^2_{|\Gamma_{CR}}dt\Bigg) \\
&\qquad + \beta(\phi_m)\int_0^T\left(\left\|e_{Rb}^M\right\|\right)^2_{L^2(\Omega_R)}dt \\
&\quad \le \beta(\phi_m)\int_0^T\left(\left\|e_{Rb}^0\right\|\right)^2_{L^2(\Omega_R)}dt. \qquad (19)
\end{aligned}$$

Taking the limit for $M \to +\infty$ and noting that the sum is bounded above, we have that

$$\lim_{k\to\infty} \left\| e_j^k \right\|_{L^2(\Omega_R)} = 0, \qquad \lim_{k\to\infty} \left\| e_j^k \right\|_{L^2((0,T);V)} = 0, \quad j = Rb, Rt. \qquad \square$$

From the boundedness of C_R^k in $\Omega_R \times (0,T)$ for all $k \geq 0$, it is then straightforward to prove that $0 \leq C_R \leq C_N$ a.e. in $\Omega_R \times (0,T)$ [14]. $\square$

Competing interests
The authors declare that they have no competing interests.

Authors' contributions
All authors contributed equally to the writing of this paper. All authors read and approved the final manuscript.

Author details
[1] Dipartimento di Matematica, Università degli Studi di Milano, Milano, Italy. [2] Dipartimento di Matematica, Politecnico di Milano, Milano, Italy.

Received: 4 February 2016 Accepted: 24 October 2016 Published online: 28 October 2016

References

1. Hughes PM, Olejnik O, Chang-Lin J-E, Wilson CG. Topical and systemic drug delivery to the posterior segments. Adv Drug Deliv Rev. 2005;57(14):2010-32.
2. El Sanharawi M, Kowalczuk L, Touchard E, Omri S, De Kozak Y, Behar-Cohen F. Protein delivery for retinal diseases: from basic considerations to clinical applications. Prog Retin Eye Res. 2010;29(6):443-65.
3. Kompella UB, Edelhauser HF. Drug product development for the back of the eye. vol. 2. New York: Springer; 2011.
4. Tsuboi S, Pederson J. Effect of plasma osmolality and intraocular pressure on fluid movement across the blood-retinal barrier. Investig Ophthalmol Vis Sci. 1988;29(11):1747-9.
5. Ethier CR, Johnson M, Ruberti J. Ocular biomechanics and biotransport. Annu Rev Biomed Eng. 2004;6:249-73.
6. Thassu D, Chader GJ. Ocular drug delivery systems: barriers and application of nanoparticulate systems. Boca Raton: CRC Press; 2012. ISBN:9781439848005.
7. Stay MS, Xu J, Randolph TW, Barocas VH. Computer simulation of convective and diffusive transport of controlled-release drugs in the vitreous humor. Pharm Res. 2003;20(1):96-102.
8. Balachandran R, Barocas VH. Computer modeling of drug delivery to the posterior eye: effect of active transport and loss to choroidal blood flow. Pharm Res. 2008;25(11):2685-96.
9. Amrite AC, Edelhauser HF, Kompella UB. Modeling of corneal and retinal pharmacokinetics after periocular drug administration. Investig Ophthalmol Vis Sci. 2008;49(1):320-32.
10. Ranta V-P, Urtti A. Transscleral drug delivery to the posterior eye: prospects of pharmacokinetic modeling. Adv Drug Deliv Rev. 2006;58(11):1164-81.
11. Ranta V-P, Mannermaa E, Lummepuro K, Subrizi A, Laukkanen A, Antopolsky M, Murtomäki L, Hornof M, Urtti A. Barrier analysis of periocular drug delivery to the posterior segment. J Control Release. 2010;148(1):42-8.
12. Ninawe PR, Hatziavramidis D, Parulekar SJ. Delivery of drug macromolecules from thermally responsive gel implants to the posterior eye. Chem Eng Sci. 2010;65(18):5170-7.
13. Mac Gabhann F, Demetriades AM, Deering T, Packer JD, Shah SM, Duh E, Campochiaro PA, Popel AS. Protein transport to choroid and retina following periocular injection: theoretical and experimental study. Ann Biomed Eng. 2007;35(4):615-30.
14. Zunino P. Mathematical and numerical modelling of mass transfer in the vascular system [PhD thesis]. Lausanne: EPFL; 2002.
15. Cliff WJ. Blood vessels. vol. 6. CUP archive; 1976. ISBN13:9780521207539.
16. Gaudana RJ, Barot M, Patel A, Khurana V, Mitra AK. Barriers for posterior segment ocular drug delivery. In: Mitra AK, editor. Treatise on ocular drug delivery. Sharjah: Bentham Science; 2013. p. 68-95. ISBN:978-1-60805-347-6.
17. Kavousanakis ME, Kalogeropoulos NG, Hatziavramidis DT. Computational modeling of drug delivery to the posterior eye. Chem Eng Sci. 2014;108:203-12.
18. Levick JR. An introduction to cardiovascular physiology. Oxford: Butterworth-Heinemann; 2013. ISBN:978-0-7506-1028-5.
19. Fung Y-C. Biomechanics: mechanical properties of living tissues. New York: Springer; 2013. ISBN-13:978-0387979472.
20. Missel PJ. Simulating intravitreal injections in anatomically accurate models for rabbit, monkey, and human eyes. Pharm Res. 2012;29(12):3251-72.
21. Kotha S, Murtomäki L. Virtual pharmacokinetic model of human eye. Math Biosci. 2014;253:11-8.
22. Raghava S, Hammond M, Kompella UB. Periocular routes for retinal drug delivery. Expert Opin Drug Deliv. 2004;1(1):99-114.
23. Ambati J, Gragoudas ES, Miller JW, You TT, Miyamoto K, Delori FC, Adamis AP. Transscleral delivery of bioactive protein to the choroid and retina. Investig Ophthalmol Vis Sci. 2000;41(5):1186-91.
24. Geroski DH, Edelhauser HF. Drug delivery for posterior segment eye disease. Investig Ophthalmol Vis Sci. 2000;41(5):961-4.
25. Pescina S, Santi P, Ferrari G, Nicoli S. Trans-scleral delivery of macromolecules. Ther Deliv. 2011;2(10):1331-49.
26. Barot M, Bagui M, Gokulgandhi MR, Mitra AK. Prodrug strategies in ocular drug delivery. Med Chem. 2012;8(4):753-68.
27. D'Amico DJ. Diseases of the retina. N Engl J Med. 1994;331:95-106.

28. Gilbarg D, Trudinger NS. Elliptic partial differential equations of second order. Grundlehren der Mathematischen Wissenschaften. vol. 224. Berlin: Springer; 2001. ISBN:978-3-642-61798-0.
29. Tojo K. A pharmacokinetic model for ocular drug delivery. Chem Pharm Bull. 2004;52(11):1290-4. doi:10.1248/cpb.52.1290.
30. Kim H, Lizak MJ, Tansey G, Csaky KG, Robinson MR, Yuan P, Wang NS, Lutz RJ. Study of ocular transport of drugs released from an intravitreal implant using magnetic resonance imaging. Ann Biomed Eng. 2005;33(2):150-64.
31. Park J, Bungay PM, Lutz RJ, Augsburger JJ, Millard RW, Roy AS, Banerjee RK. Evaluation of coupled convective-diffusive transport of drugs administered by intravitreal injection and controlled release implant. J Control Release. 2005;105(3):279-95.
32. Haghjou N, Abdekhodaie M, Cheng Y, Saadatmand M. Computer modeling of drug distribution after intravitreal administration. World Acad Sci, Eng Tecnol. 2011;53:706-16.

Submit your manuscript to a SpringerOpen journal and benefit from:

► Convenient online submission
► Rigorous peer review
► Immediate publication on acceptance
► Open access: articles freely available online
► High visibility within the field
► Retaining the copyright to your article

Submit your next manuscript at ► springeropen.com